1-1-2020

Thermionic emission in nodal-ring semimetals

Suguo Chen
suguo@uow.edu.au

Sunchao Huang
sh676@uowmail.edu.au

Wenye Duan

Wei Shi

C Zhang
University of Wollongong, czhang@uow.edu.au

Thermionic emission in nodal-ring semimetals

Abstract

© 2020 Author(s). We theoretically investigate the thermionic emission from nodal-ring semimetals. The thermionic emission is found to be anisotropic in the x- and y-directions. The anisotropic emission can be enhanced by increasing the radius of nodal-ring b. The main feature of nodal-ring semimetals not only results in anisotropic thermionic emission but also affects the value of thermionic emission current density (TECD). The TECD of the lower branch of the energy-momentum dispersion increases with b, while the TECD of the upper branch decreases with b. Unlike in conventional materials, the TECD in nodal-ring semimetals depends on Fermi energy that is similar to the situation in Dirac semimetals. The underlined reason is that Dirac semimetals and nodal-ring semimetals have a linear or a linear-like energy-momentum dispersion while conventional materials have a parabolic energy-momentum dispersion. The TECD of nodal-ring semimetals depends strongly on work function and temperature.

Disciplines

Engineering | Science and Technology Studies

Publication Details

Chen, S., Huang, S., Duan, W., Shi, W. & Zhang, C. (2020). Thermionic emission in nodal-ring semimetals. Journal of Applied Physics, 128 (6),

Journal of Applied Physics

Thermionic emission in nodal-ring semimetals

Cite as: J. Appl. Phys. **128**, 065108 (2020); https://doi.org/10.1063/5.0007139
Submitted: 11 March 2020 . Accepted: 29 July 2020 . Published Online: 13 August 2020

Suguo Chen, Sunchao Huang, Wenye Duan, Wei Shi, and Chao Zhang

AIP Publishing

Journal of Applied Physics ARTICLE scitation.org/journal/jap

Thermionic emission in nodal-ring semimetals

Cite as: J. Appl. Phys. **128**, 065108 (2020); doi: 10.1063/5.0007139
Submitted: 11 March 2020 · Accepted: 29 July 2020 ·
Published Online: 13 August 2020

Suguo Chen,[1] Sunchao Huang,[2] Wenye Duan,[3] Wei Shi,[1] and Chao Zhang[2,a)]

AFFILIATIONS

[1]Department of Applied Physics, Xian University of Technology, Xian 710048, China
[2]School of Physics, University of Wollongong, Northfield Avenue, Wollongong, New South Wales 2522, Australia
[3]School of Science, East China University of Science and Technology, Shanghai 200237, China

[a)]**Author to whom correspondence should be addressed:** czhang@uow.edu.au

ABSTRACT

We theoretically investigate the thermionic emission from nodal-ring semimetals. The thermionic emission is found to be anisotropic in the x- and y-directions. The anisotropic emission can be enhanced by increasing the radius of nodal-ring b. The main feature of nodal-ring semimetals not only results in anisotropic thermionic emission but also affects the value of thermionic emission current density (TECD). The TECD of the lower branch of the energy–momentum dispersion increases with b, while the TECD of the upper branch decreases with b. Unlike in conventional materials, the TECD in nodal-ring semimetals depends on Fermi energy that is similar to the situation in Dirac semimetals. The underlined reason is that Dirac semimetals and nodal-ring semimetals have a linear or a linear-like energy–momentum dispersion while conventional materials have a parabolic energy–momentum dispersion. The TECD of nodal-ring semimetals depends strongly on work function and temperature.

I. INTRODUCTION

Materials with a linear energy–momentum dispersion, such as graphene,[1] Dirac semimetals,[2] and Weyl semimetals,[3,4] have received much attention in recent years.[5–10] Graphene, a one-layer atomically thin material, has many unique properties such as universal optical conductivity,[11] ultrahigh electronic mobility ($\sim$200 000 cm^2 V^{-1} s^{-1}),[12] and Dirac-like electrons.[13] Dirac semimetals host massless electrons described by the Dirac equation, which are protected by the time-reversal and spatial inversion symmetries.[14] If one of the above symmetries is broken, Dirac semimetals turn to Weyl semimetals.[15] Recently, new types of 3D topological materials, nodal-line semimetals, have been theoretically predicted[16–18] and experimentally realized in ZrSiSe.[19] Nodal-ring (nodal-line) semimetals are protected not only by the time-reversal and the inversion symmetries[20] but also by mirror reflection and nonsymmorphic symmetries.[21,22] Their conduction and valence bands cross each other at many points, forming a continuous ring. The radius of the ring (b) is a key material parameter, which can be measured by angle-resolved photoemission spectroscopy.[23] However, direct physical properties measurement associated with b is highly desired. A magneto-optical way to determine b accurately has been proposed recently.[24] By applying a magnetic field along the ring axis, the axial magneto-optical response is found to have a giant peak at the position of $2b$, which is independent of the strength of the magnetic field and can be used to determine the value of b. Magnetic susceptibility,[25] Landau quantization,[26] Lifshitz transitions,[27] and quantum anomalies[28–31] have been investigated in nodal-ring systems.

In the present work, we shall investigate thermionic emission in such a system. Thermionic emission is a fundamental process where electrons are driven by thermal energy to escape from bulk states, which has been extensively studied in conventional semiconductors with a parabolic energy–momentum dispersion due to its potential applications in thermionic devices such as refrigerators and energy generators.[32–34] The practical applications of thermionic devices are hindered by the lack of low work-function materials[35] and the space charge effect.[36] Thermionic emission receives increasing attention,[37–43] thanks to the technology developments in obtaining low work-function materials and the discovery of new materials such as graphene and Dirac semimetals.[44–48] For conventional semiconductors, the thermionic emission current density (TECD) is described by the Richardson–Dushman law[32] $J_{RD} = A_{RD}T^2\,\mathrm{e}^{-\mathrm{W}/\mathrm{k_B T}}$, where $A_{RD} = \frac{qmk_B^2}{2\pi^2\hbar^3} = 1.2 \times 10^6$ A m^{-2} K^{-2}, q is the absolute charge of an electron, m is the mass of an electron, k_B is the Boltzmann constant, $\hbar$ is the reduced Plank constant, T is the dynamical temperature, and W is the work function.[35] For 3D

Dirac semimetals, we found in this work that the TECD is given by $J_D = A_D T^2 e^{-W/k_B T}$, where $A_D = \frac{qk_B^2}{4\pi^2\hbar^3 v_F^2}(W+E_F+2k_BT)$. A_D is smaller than A_{RD}. The underlying reason is that the density of states of 3D semimetals $g(\epsilon) = \frac{\epsilon^2}{\pi^2\hbar^3 v_F^3}$[49] is smaller than that of 3D conventional semiconductors $g(\epsilon) = \frac{(2m)^{3/2}}{2\pi^2\hbar^3}\sqrt{\epsilon}$. Although A_D is smaller than A_{RD}, the thermionic emission in Dirac systems has one fundamental advantage that the average energy carried by one freedom of electrons in Dirac systems is twice of that in conventional semiconductors.[41,50]

In this work, we study the thermionic emission in 3D nodal-ring semimetals. In the low energy regime, the density of states of nodal-ring semimetals is larger than that of 3D Dirac semimetals. Additionally, the low energy–momentum in nodal-ring semimetals is anisotropic in the x- and y-directions. These features make the TECD of nodal-ring semimetals different from its previous counterparts. In Sec. II, we develop the necessary formulas to describe the density of states and the TECD. Section III discusses thermionic emission in different situations.

II. FORMALISM

The energy–momentum dispersion of nodal-ring semimetals is given as[51]

$$\epsilon = s\hbar v_F\sqrt{k_x^2 + (k_\perp + s'b)^2}, \tag{1}$$

where $s = \pm$ and $s' = \pm$ are the band indexes and $k_\perp = \sqrt{k_y^2 + k_z^2}$. The band structure of nodal-ring semimetals is plotted in Fig. 1 according to Eq. (1), where $k_x = 0$, $\epsilon_0 = \hbar v_F b$ and the dashed horizontal line is the Fermi level. We label the two conduction bands as lower branch ϵ_1 ($s = +, s' = -$) and upper branch ϵ_2 ($s = +, s' = +$), and valance band as ϵ_3 ($s = -, s' = -$) and ϵ_4 ($s = -, s' = +$), respectively. The conduction band ϵ_1 touches the valence band ϵ_3 at points ($k_x = 0$ and $k_\perp = b$) forming a nodal-ring in the k_y–k_z plane, and the radius of the ring is b, which results in an anisotropic energy dispersion along the k_x and k_y directions and an isotropic energy dispersion along the k_y and k_z directions. The minimum value of ϵ_2 is ϵ_0, which means there is no density of states for ϵ_2 when $\epsilon_2 < \epsilon_0$. Here, we only investigate the thermionic emission in conduction bands ϵ_1 and ϵ_2 since the energy of ϵ_3 and ϵ_4 is less than $W + E_F$ and make no contribution to thermionic emission.

The TECD in the m direction ($m = x$ or y) and n band ($n = 1$ or 2) is calculated by

$$J_{m,n} = \frac{2}{(2\pi)^3}\int q v_{m,n}(\epsilon) f(\epsilon - E_F)\mathrm{d}k_x\mathrm{d}k_y\mathrm{d}k_z, \tag{2}$$

where 2 is the spin factor, $f(\epsilon - E_F)$ is the Fermi–Dirac distribution function, q is the charge of electron, and $v_{m,n}$ is the velocity component in the m direction for n band, which is calculated by

$$v_{m,n} = \frac{1}{\hbar}\frac{\partial\epsilon_n}{\partial k_m}. \tag{3}$$

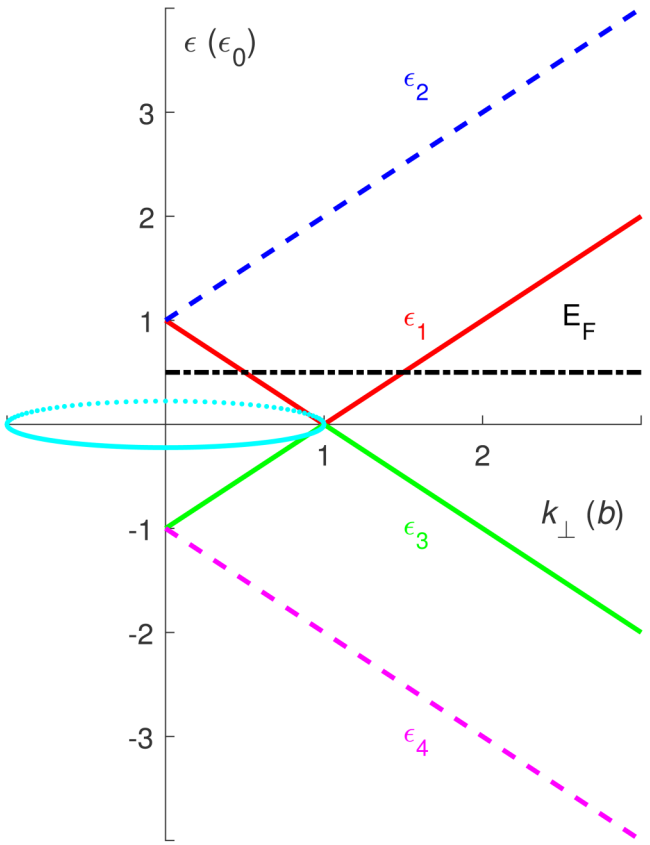

FIG. 1. The energy–momentum dispersion of nodal-ring semimetals plotted by using Eq. (1), where $k_x = 0$, $k_\perp = \sqrt{k_y^2 + k_z^2}$, and $\epsilon_0 = \hbar v_F b$.

The energy dispersion is isotropic in the k_y and k_z directions, which results in the same TECD and the same form of energy due to the momentum component in the y- and z-directions. Therefore, only the TECD in the x- and y-directions needs to be calculated. In the integral, k_x, k_y, and k_z should make $\epsilon_{m,n} \geq W + E_F$ so that we only count the electrons that have enough energy to overcome the surface barrier in the m direction.

Unlike a parabolic dispersion, the energy dispersion $\epsilon = \hbar v_F k$ cannot be easily separated into three directions. To proceed with our analysis of determining minimum energy in a given direction, we need to decompose the energy along with three directions in a reasonable way. For a Dirac system, $\epsilon = \hbar v_F\sqrt{k_x^2 + k_y^2 + k_z^2} = \hbar v_F\frac{k_x^2+k_y^2+k_z^2}{\sqrt{k_x^2+k_y^2+k_z^2}}$. We then decompose them along different directions as $\epsilon_x = \hbar v_F\frac{k_x^2}{k}$, $\epsilon_y = \hbar v_F\frac{k_y^2}{k}$, and $\epsilon_z = \hbar v_F\frac{k_z^2}{k}$. In the limiting case $k_y = k_z = 0$, the energy is given as $\epsilon_x = \hbar v_F\frac{k_x^2}{k} = \hbar v_F k$. The above result can also be equivalently obtained by using the velocity $v_i = \frac{\partial\epsilon}{\hbar\partial k_i} = v_F\frac{k_i}{k}$, where $i = x, y$, and z. The energy along each direction is given as $\epsilon_x = \hbar v_x k_x = \hbar v_F\frac{k_x^2}{k}$,

$\epsilon_y = \hbar v_F \frac{k_y^2}{k}$, and $\epsilon_z = \hbar v_F \frac{k_z^2}{k}$. Due to this equivalence of the two methods, we use the velocity approach for nodal-ring systems in assigning energies along with three directions. For the nodal-ring system, band 1 is made up of many Dirac cones and the origin of the Dirac cones is $(0, \frac{k_y b}{k_\perp}, \frac{k_z b}{k_\perp})$ instead of (0,0,0) in Dirac materials. Its energy due to the momentum component is written as

$$\epsilon_{x,1} = \hbar k_x v_{x,1} = \frac{\hbar v_F k_x^2}{M_1}, \tag{4}$$

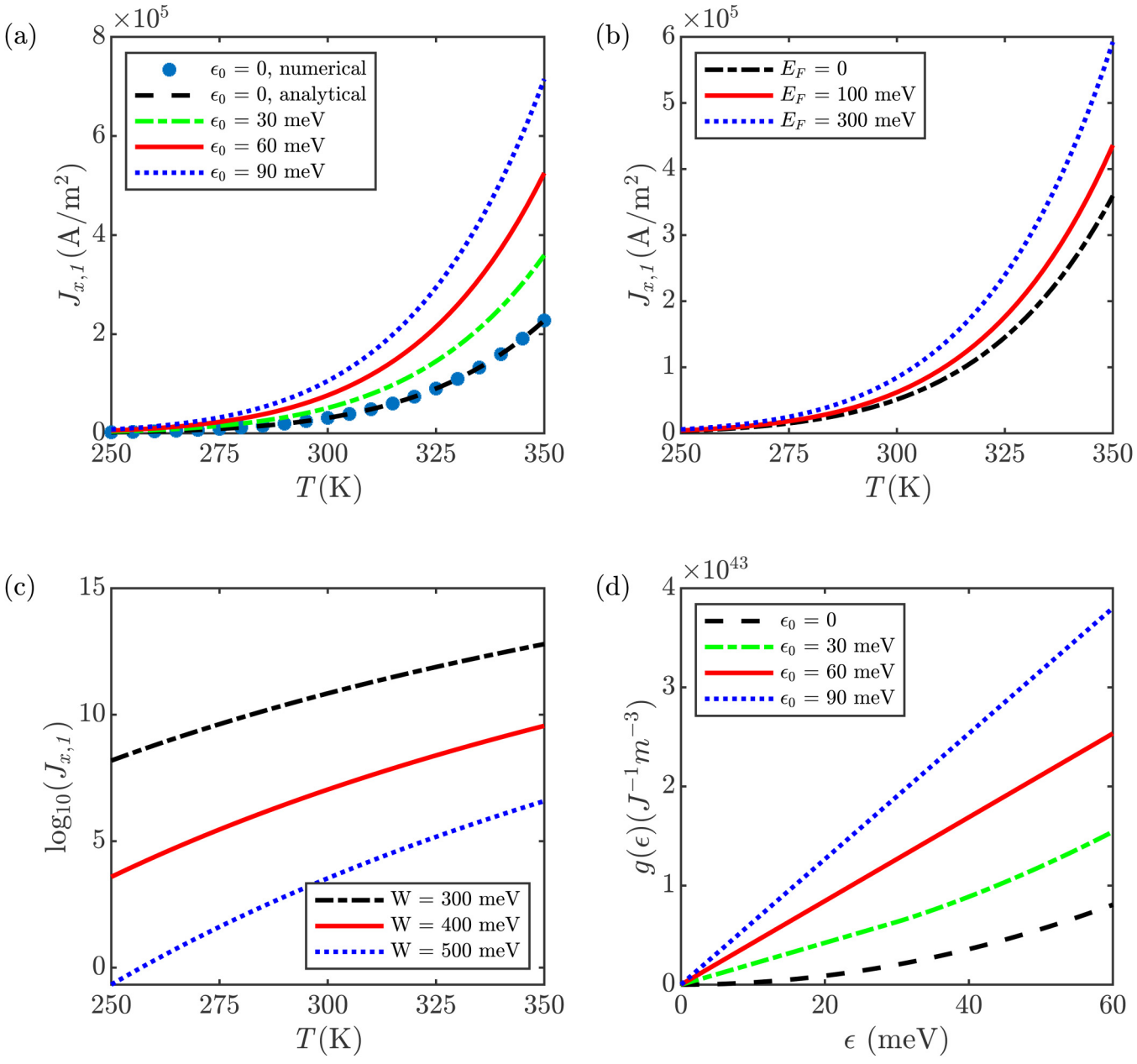

FIG. 2. Thermionic emission of ϵ_1. (a) Temperature dependence of $J_{x,1}$ at four values of ϵ_0 from 0 to 90 meV. For the limit $\epsilon_0 = 0$, $J_{x,1}$ is obtained both analytically and numerically and the results agree with each other perfectly, where $W = 300$ meV and $E_F = 0$. (b) Temperature dependence of $J_{x,1}$ at three values of E_F from 0 to 300 meV, where $W = 300$ meV and $\epsilon_0 = 30$ meV. (c) $\log_{10}(J_{x,1})$ as a function of T at three values of W, where $\epsilon_0 = 30$ meV and $E_F = 0$. (d) Density of states of band 1 against ϵ at four values of ϵ_0 that is numerically calculated according to $g(\epsilon) = \frac{2}{V}\sum_k \delta(\epsilon - \epsilon_k)$, where 2 is the spin factor.

$$\epsilon_{y,1} = \hbar\left(k_y - \frac{k_y b}{k_\perp}\right)v_{y,1} = \frac{\hbar v_F}{M_1}\left(k_y^2 - \frac{2bk_y^2}{k_\perp} + \frac{bk_y^2}{k_\perp^2}\right), \quad (5)$$

$$\epsilon_{z,1} = \hbar\left(k_z - \frac{k_z b}{k_\perp}\right)v_{z,1} = \frac{\hbar v_F}{M_1}\left(k_z^2 - \frac{2bk_z^2}{k_\perp} + \frac{bk_z^2}{k_\perp^2}\right), \quad (6)$$

where $M_1 = \sqrt{k_x^2 + (k_\perp - b)^2}$. Similarly, the energy due to the momentum component of band 2 is given as

$$\epsilon_{x,2} = \hbar k_x v_{x,2} = \frac{\hbar v_F k_x^2}{M_2}, \quad (7)$$

$$\epsilon_{y,2} = \hbar\left(k_y + \frac{k_y b}{k_\perp}\right)v_{y,2} = \frac{\hbar v_F}{M_2}\left(k_y^2 + \frac{2bk_y^2}{k_\perp} + \frac{bk_y^2}{k_\perp^2}\right), \quad (8)$$

$$\epsilon_{z,2} = \hbar(k_z + \frac{k_z b}{k_\perp})v_{z,2} = \frac{\hbar v_F}{M_2}\left(k_z^2 + \frac{2bk_z^2}{k_\perp} + \frac{bk_z^2}{k_\perp^2}\right), \quad (9)$$

where $M_z = \sqrt{k_x^2 + (k_\perp + b)^2}$. It is easy to see that $\epsilon_{x,1} + \epsilon_{y,1} + \epsilon_{z,1} = \frac{\hbar v_F}{M_1}(k_x^2 + k_\perp^2 - 2bk_\perp + b^2) = \epsilon_1$ and $\epsilon_{x,2} + \epsilon_{y,2} + \epsilon_{z,2} = \frac{\hbar v_F}{M_2}(k_x^2 + k_\perp^2 + 2bk_\perp + b^2) = \epsilon_2$. In our calculations, the Fermi velocity v_F is set to 10^6 m/s.

III. THERMIONIC EMISSION

In the present work, we first study TECD of band 1 and 2 separately and then add them together since TECD of band 1 at the limit of $\epsilon_0 = 0$ can be analytically obtained that helps to verify our results. Additionally, TECD of bands 1 and 2 has a different response to the radius of nodal-ring. Now, we consider the limit $\epsilon_0 = 0$, i.e., $b = 0$ where the energy dispersion of band 1 becomes $\epsilon_1 = \hbar v_F k$ which is the energy–momentum of 3D Dirac semimetals.[7] In this case, x, y, and z directions have the same TECD and can be analytically obtained as

$$J_{x,1} = J_{y,1} = J_{z,1} = \frac{2}{(2\pi)^3}\iiint qf(\epsilon)v_{z,1}\mathrm{d}k_x\mathrm{d}k_y\mathrm{d}k_z, \quad (10)$$

where $v_{z,1} = \frac{\partial(\hbar v_F k)}{\hbar \partial k_z} = v_F\frac{k_z}{k} = v_F\cos(\theta)$ should make $\epsilon_{z,1} \geq E_F + W$, i.e., $\epsilon_{z,1} = \hbar k_z v_{z,1} = \hbar v_F k\cos^2(\theta) \geq E_F + W$ resulting in $\cos^2(\theta_{\max}) = \frac{k_{\min}}{k}$ with $k_{\min} = \frac{E_F + W}{\hbar v_F}$, θ is the angle between $k_{z,1}$ and k. Since $\epsilon_1 - E_F \geq \epsilon_{z,1} - E_F \geq W$, where $W = 300$ meV, the Fermi–Dirac distribution function can be replaced by the Maxwell–Boltzmann distribution function $f(\epsilon_1) = \frac{1}{1+e^{(\epsilon_1 - E_F)/k_B T}} \approx e^{(E_F - \epsilon_1)/k_B T}$ for $T = 350$ K ($k_B T \approx 30$ meV). The integral can be evaluated in spherical coordinates,

$$J_{x,1} = \frac{q}{4\pi^3}\int_{k_{\min}}^{+\infty}\int_0^{\theta_{\max}}\int_0^{2\pi} e^{(E_F - \epsilon_1)/k_B T} v_F\cos(\theta)k^2\sin(\theta)\mathrm{d}\phi\mathrm{d}\theta\mathrm{d}k$$
$$= \frac{qk_B^2}{4\pi^2\hbar^3 v_F^2}(W + E_F + 2k_B T)T^2 e^{-W/k_B T}. \quad (11)$$

The analytical and numerical results are shown by a black dashed curve and solid circles in Fig. 2(a), respectively, which agree with each other. When $\epsilon_0 \neq 0$, the TECD is calculated numerically by using Eqs. (2)–(9), and the results at three values of ϵ_0 are plotted in Fig. 2(a), which indicates that the TECD can be enhanced by ϵ_0. A large ϵ_0 means a large nodal-ring, which results in a large density of states [shown in Fig. 2(d)]. This is the underlying reason for the increase of the TECD.

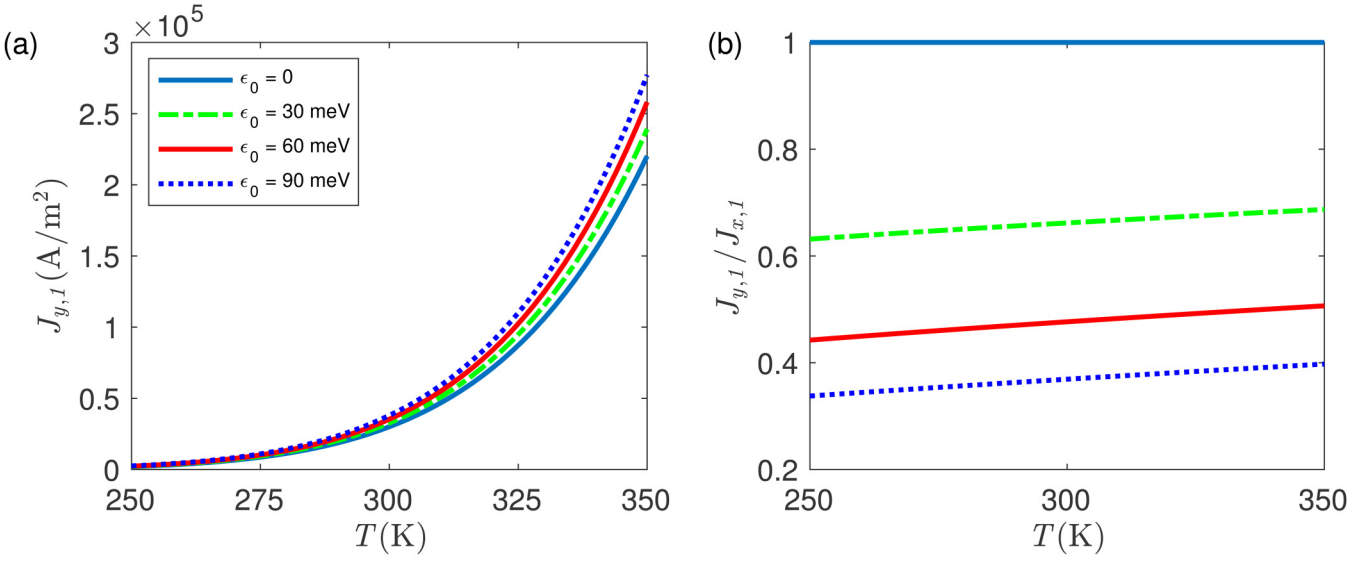

FIG. 3. The TECD in the ϵ_1 band. (a) $J_{y,1}$ and (b) $J_{y,1}/J_{x,1}$ as a function of T at four values of ϵ_0 from 0 to 90 meV.

The TECD depends on Fermi energy (E_F) through the density of states. The thermionic properties of a material are determined by the electrons near the Fermi level since they are more active and energetic. Electrons near the Fermi level have higher average energy, which results in a higher chance to escape from the material. When E_F is increased by doping or an external voltage, there are more electrons near the Fermi level because the density of states increases with the energy [see Fig. 2(d)]. Temperature dependence of TECD at three values of E_F is shown in Fig. 2(b). At a fixed temperature, the TECD increases with E_F.

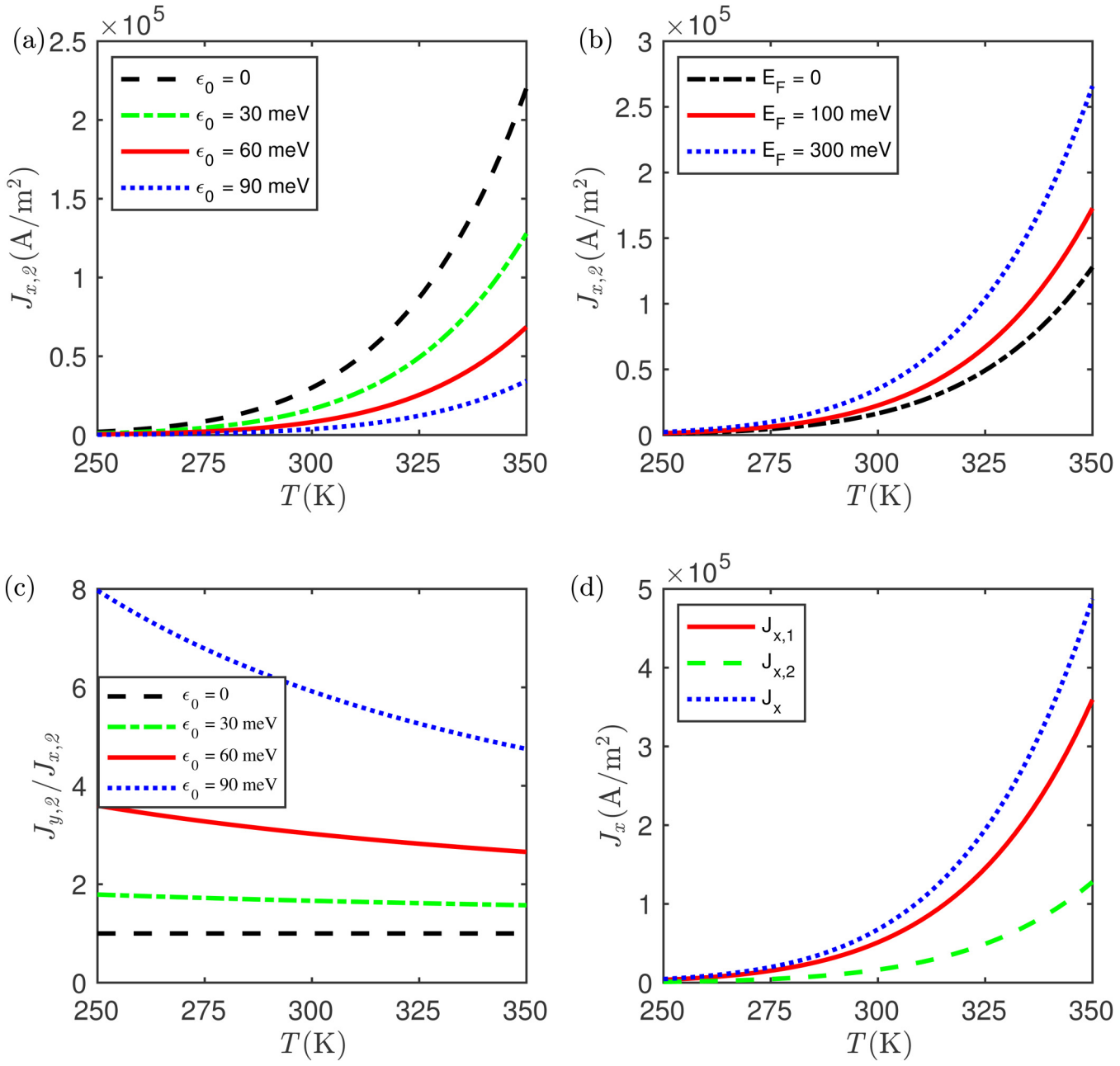

FIG. 4. Thermionic emission of the upper branch. (a) Temperature dependence of $J_{x,2}$ at four values of ϵ_0 from 0 to 90 meV. (b) Temperature dependence of $J_{x,2}$ at three values of E_F. (c) $J_{y,2}/J_{x,2}$ against T at three values of ϵ_0. (d) $J_{x,1}$, $J_{x,2}$, and J_x as a function of T, where $\epsilon_0 = 30$ meV.

In a thermionic process, electrons gain thermal energy to overcome the surface barrier. In this sense, the TECD is dependent on the height of the surface barrier, i.e., work function W and temperature. Equation (11) shows that $J_{x,1}$ decreases with W exponentially when $\epsilon = 0$. When $\epsilon_0 \neq 0$, the decrease still exists, shown in Fig. 2(c). For $T = 250$ K, $J_{x,1}$ drops nearly five orders when W changes from 300 meV to 400 meV. When the temperature is increased from 250 K to 350 K, the dropping tendency slows down slightly. Increasing temperature means more electrons have sufficient energy to overcome the surface barrier.

Overall, the TECD depends on E_F and ϵ_0 weakly. However, the TECD depends strongly on W and T. In a practical application, the working temperature is fixed in a specific range and a minimum TECD, usually in the order of 10 000 A/m^2, is required.[35] For example, the working temperature is around 250−320 K when thermionic effect is employed to make air-conditions and refrigerators. This is why our discussion is mainly focused on 250−350 K. The temperature is around 500−1000 K when the thermionic effect is employed to harvest thermal heat. In this sense, a proper work function should be chosen according to the working temperature and the minimum TECD. In a thermionic refrigerator, the work function usually needs to be less than 300 meV.[32]

Similar to $J_{x,1}$, $J_{y,1}$ also can be enhanced by ϵ_0, shown in Fig. 3(a). The energy–momentum dispersion of nodal-ring systems is anisotropic in the x- and y-directions shown in Eq. (1). This results in that the thermionic emission is different in the x- and y-directions. To see the anisotropic thermionic emission, $J_{y,1}$ and $J_{y,1}/J_{x,1}$ as a function of T are calculated and shown in Fig. 3(b). In the limit $\epsilon_0 = 0$, the value of $J_{y,1}/J_{x,1}$ is equal to one in the whole temperature range. Indeed, this is the real situation since the thermionic emission is isotropic in Dirac systems ($\epsilon_0 = 0$). For $T = 250$ K, $J_{y,1}/J_{x,1}$ decreases with ϵ_0 and the minimum value reaches 0.35, indicating anisotropic thermionic emission. The value of $J_{y,1}/J_{x,1}$ increases with T, which indicates J_y and J_x having different temperature dependence.

Now, we discuss the thermionic emission of the upper branch ϵ_2. The thermionic emission current $J_{x,2}$ as a function of T at four values of ϵ_0 is plotted in Fig. 4(a). The results are fundamentally different from the results of the lower branch. $J_{x,2}$ decreases with ϵ_0, while $J_{x,1}$ increases with ϵ_0. The decrement also can be understood by the decrease in the density of states. For the upper branch, the density of states is zero when $\epsilon < \epsilon_0$. In this sense, the density of states near to the Fermi surface ($E_F = 0$) decreases with ϵ_0, which leads to the number of the thermally driven electrons decreasing with ϵ_0 and the decrease of $J_{x,2}$. For $T = 350$ K, the value of $J_{x,2}$ drops more than sixfold when ϵ_0 changes from 0 to 90 meV. Besides, the zero density of states results in a smaller $J_{x,2}$ compared with $J_{x,1}$. To visualize this, $J_{x,1}$ and $J_{x,2}$ together with $J_x = J_{x,1} + J_{x,2}$ as a function of T is plotted in Fig. 4(d). The results show that $J_{x,2}$ is considerably smaller than $J_{x,1}$. This indicates that the total TECD is mainly contributed by the lower branch. For example, $J_{x,1}$ contributes about 75% to J_x when $T = 350$ K and $\epsilon_0 = 30$ meV.

Fermi energy dependent on $J_{x,2}$ is investigated and shown in Fig. 4(b). The results are similar to that in the lower branch, i.e., $J_{x,2}$ increases with E_F. When E_F is increased, the density of states near the Fermi surface increases and the $J_{x,2}$ is enhanced. For the upper branch, the anisotropic thermionic emission is expected due to the anisotropy of energy–momentum dispersion. Temperature dependence of $J_{y2}/J_{x,2}$ at four values of ϵ_0 is plotted in Fig. 4(c). In the limit of $\epsilon_0 = 0$, $J_{y2}/J_{x,2}$ is equal to one, which is rather reasonable since thermionic emission in Dirac systems is isotropic. When ϵ_0 is increased, $J_{y2}/J_{x,2}$ is larger than one showing anisotropic thermionic emission in the x- and y-directions. Additionally, the anisotropic emission increases with ϵ_0.

IV. CONCLUSION

We have investigated thermionic emission in nodal-ring systems. The thermionic emission shows anisotropy in the x- and y-directions in both the lower and upper branches of energy–momentum dispersion. The anisotropic emission can be enhanced by increasing ϵ_0. The TECD increases with ϵ_0 in the lower branch, while it decreases with ϵ_0 in the upper branch. However, the TECD increases with E_F for both bands. Although the value of TECD can be tuned by E_F and ϵ_0, the change is limited within an order of magnitude. T and W can significantly change the value of TECD. If material parameters such as W, E_F, and v_F have the same values, TECD of nodal-ring systems is larger than that in Dirac systems due to their larger density of states. Our results are helpful to understand the thermionic emission in nodal-ring systems.

We would like to note that although TECD is dependent on the ring radius, the radius is normally difficult to be varied. For some nodal-ring semi-metals, the ring property is dependent on the magnetic field. One possible way to vary b is to attach a ferromagnetic layer to the device and the magnetic field effect can be controlled by temperature, and in turn, the radius can be varied in a certain range.[52]

ACKNOWLEDGMENTS

The work was supported by the Australian Research Council Grant (DP160101474), the National Natural Science Foundation of China (NNSFC) (Nos. 11704310 and 61975163), and the Natural Science Foundation of Shaanxi Provincial Department of Education (No. 17JK0541).

DATA AVAILABILITY

The data that support the findings of this study are available from the corresponding author upon reasonable request.

REFERENCES

[1] A. K. Geim and K. S. Novoselov, in *Nanoscience and Technology: A Collection of Reviews from Nature Journals* (World Scientific, 2010), p. 11.
[2] Y. Chen, J. G. Analytis, J.-H. Chu, Z. Liu, S.-K. Mo, X.-L. Qi, H. Zhang, D. Lu, X. Dai, Z. Fang *et al.*, Science **325**, 178 (2009).
[3] B. Lv, H. Weng, B. Fu, X. Wang, H. Miao, J. Ma, P. Richard, X. Huang, L. Zhao, G. Chen *et al.*, Phys. Rev. X **5**, 031013 (2015).
[4] A. Burkov and L. Balents, Phys. Rev. Lett. **107**, 127205 (2011).
[5] S. Huang, M. Sanderson, J. Tian, Q. Chen, F. Wang, and C. Zhang, J. Phys. D Appl. Phys. **51**, 015101 (2017).
[6] C. Zhu, F. Wang, Y. Meng, X. Yuan, F. Xiu, H. Luo, Y. Wang, J. Li, X. Lv, L. He *et al.*, Nat. Commun. **8**, 14111 (2017).
[7] R. Lundgren and G. A. Fiete, Phys. Rev. B **92**, 125139 (2015).
[8] S. Huang, M. H. Tran, J. Zuber, Q. Wang, Y. Zhu, and C. Zhang, J. Opt. Soc. Am. B **36**, 200 (2019).

[9]J. Viljas and T. Heikkilä, Phys. Rev. B **81**, 245404 (2010).
[10]M. Sanderson, S. Huang, Q. Bao, and C. Zhang, J. Phys. D Appl. Phys. **50**, 385301 (2017).
[11]V. Gusynin, S. Sharapov, and J. Carbotte, New J. Phys. **11**, 095013 (2009).
[12]K. I. Bolotin, K. Sikes, Z. Jiang, M. Klima, G. Fudenberg, J. Hone, P. Kim, and H. Stormer, Solid State Commun. **146**, 351 (2008).
[13]A. K. Geim, Science **324**, 1530 (2009).
[14]Z. Wang, Y. Sun, X.-Q. Chen, C. Franchini, G. Xu, H. Weng, X. Dai, and Z. Fang, Phys. Rev. B **85**, 195320 (2012).
[15]A. Zyuzin, S. Wu, and A. Burkov, Phys. Rev. B **85**, 165110 (2012).
[16]A. Burkov, M. Hook, and L. Balents, Phys. Rev. B **84**, 235126 (2011).
[17]X. Zhang, Z.-M. Yu, X.-L. Sheng, H. Y. Yang, and S. A. Yang, Phys. Rev. B **95**, 235116 (2017).
[18]L. S. Xie, L. M. Schoop, E. M. Seibel, Q. D. Gibson, W. Xie, and R. J. Cava, APL Mater. **3**, 083602 (2015).
[19]J. Hu, Z. Tang, J. Liu, X. Liu, Y. Zhu, D. Graf, K. Myhro, S. Tran, C. N. Lau, J. Wei *et al.*, Phys. Rev. Lett. **117**, 016602 (2016).
[20]Y. Kim, B. J. Wieder, C. Kane, and A. M. Rappe, Phys. Rev. Lett. **115**, 036806 (2015).
[21]J. Liu, D. Kriegner, L. Horak, D. Puggioni, C. R. Serrao, R. Chen, D. Yi, C. Frontera, V. Holy, A. Vishwanath *et al.*, Phys. Rev. B **93**, 085118 (2016).
[22]S.-Y. Yang, H. Yang, E. Derunova, S. S. Parkin, B. Yan, and M. N. Ali, Adv. Phys. X **3**, 1414631 (2018).
[23]L. M. Schoop, M. N. Ali, C. Straßer, A. Topp, A. Varykhalov, D. Marchenko, V. Duppel, S. S. Parkin, B. V. Lotsch, and C. R. Ast, Nat. Commun. **7**, 11696 (2016).
[24]W. Duan, C. Yang, Z. Ma, Y. Zhu, and C. Zhang, Phys. Rev. B **99**, 045124 (2019).
[25]M. Koshino and I. F. Hizbullah, Phys. Rev. B **93**, 045201 (2016).
[26]J.-W. Rhim and Y. B. Kim, Phys. Rev. B **92**, 045126 (2015).
[27]H. Jiang, L. Li, J. Gong, and S. Chen, Eur. Phys. J. B **91**, 75 (2018).
[28]A. Burkov, Phys. Rev. B **97**, 165104 (2018).
[29]Y. Sun, Y. Zhang, C.-X. Liu, C. Felser, and B. Yan, Phys. Rev. B **95**, 235104 (2017).
[30]J. Liu and L. Balents, Phys. Rev. B **95**, 075426 (2017).
[31]S. T. Ramamurthy and T. L. Hughes, Phys. Rev. B **95**, 075138 (2017).
[32]G. Mahan, J. Sofo, and M. Bartkowiak, J. Appl. Phys. **83**, 4683 (1998).
[33]B. Lough, S. Lee, Z. Dou, R. Lewis, and C. Zhang, Physica E **17**, 651 (2003).
[34]M. F. O'Dwyer, R. Lewis, C. Zhang, and T. Humphrey, Phys. Rev. B **72**, 205330 (2005).
[35]G. Mahan, J. Appl. Phys. **76**, 4362 (1994).
[36]I. Langmuir, Phys. Rev. **2**, 450 (1913).
[37]M. Trushin, Phys. Rev. B **97**, 195447 (2018).
[38]S.-J. Liang, B. Liu, W. Hu, K. Zhou, and L. Ang, Sci. Rep. **7**, 46211 (2017).
[39]D. M. Trucchi, A. Bellucci, M. Girolami, P. Calvani, E. Cappelli, S. Orlando, R. Polini, L. Silvestroni, D. Sciti, and A. Kribus, Adv. Energy Mater. **8**, 1802310 (2018).
[40]X. Zhang, Y. Pan, and J. Chen, IEEE Trans. Electron Devices **64**, 4594 (2017).
[41]X. Zhang, W. Peng, G. Su, S. Su, and J. Chen, J. Phys. D Appl. Phys. **51**, 405501 (2018).
[42]Y. S. Ang, Y. Chen, C. Tan, and L. Ang, Phys. Rev. Appl. **12**, 014057 (2019).
[43]M. Trushin, Appl. Phys. Lett. **112**, 171109 (2018).
[44]F. Jin and D. Carter, J. Vac. Sci. Technol. B **36**, 051804 (2018).
[45]F. Jin and A. Beaver, J. Vac. Sci. Technol. B **35**, 041202 (2017).
[46]Y. Ang, S.-J. Liang, and L. Ang, MRS Bull. **42**, 505 (2017).
[47]F. Zhu, X. Lin, P. Liu, K. Jiang, Y. Wei, Y. Wu, J. Wang, and S. Fan, Nano Res. **7**, 553 (2014).
[48]F. Morini, E. Dubois, J.-F. Robillard, S. Monfray, and T. Skotnicki, Phys. Status Solidi (a) **211**, 1334 (2014).
[49]S. D. Sarma, E. Hwang, and H. Min, Phys. Rev. B **91**, 035201 (2015).
[50]S. Huang, M. Sanderson, Y. Zhang, and C. Zhang, Appl. Phys. Lett. **111**, 183902 (2017).
[51]S. Mukherjee and J. Carbotte, Phys. Rev. B **95**, 214203 (2017).
[52]R. Chen, Z. Chen, X.-Y. Song, J. Schneeloch, G. Gu, F. Wang, and N. Wang, Phys. Rev. Lett. **115**, 176404 (2015).